Plant Physiology®

Plant Physiology, 2024, **195**, 2520–2523
https://doi.org/10.1093/plphys/kiae221
Advance access publication 22 April 2024
Letter

Imaging of labile Fe^{2+} and Fe^{3+} in living *Arabidopsis thaliana* roots

Carine Alcon,[1] Arnaud Comte,[2] Catherine Curie,[1] and Tou Cheu Xiong[1]*

[1]IPSiM, Univ Montpellier, CNRS, INRAE, Montpellier, France
[2]Univ Lyon, Université Claude Bernard Lyon 1, Villeurbanne, France
*Author for correspondence: tou-cheu.xiong@inrae.fr
The author responsible for distribution of materials integral to the findings presented in this article in accordance with the policy described in the Instructions for Authors (https://academic.oup.com/plphys/pages/General-Instructions) is Tou Cheu Xiong (tou-cheu.xiong@inrae.fr).

Dear Editor,

Imaging of iron (Fe) in living organisms is challenging, and ways to visualize Fe are limited to sophisticated elemental methods and/or fixed tissues. As a transition metal, Fe cycles between 2 oxidation states, Fe^{2+} and Fe^{3+}, losing or donating an electron in doing so. This property enables Fe to participate in key metabolic pathways (Briat et al. 2015). Imaging of the redox species of Fe is therefore of interest to decipher its biological functions. Cellular Fe is partitioned into 2 distinct pools (Koppenol and Hider 2019): static Fe, which is tightly bound to its ligands, and labile Fe, which is weakly bound and can be exchanged between ligands rather effortlessly. To date, there are no reports describing the distribution of Fe^{2+} and Fe^{3+} labile pools in living organisms. The Perls-DAB histochemical method stains Fe in fixed tissues, chiefly the Fe^{3+} form (Roschzttardtz et al. 2009), but it mainly detects the static Fe fraction since labile Fe is likely lost during tissue fixation. In order to address the dynamics of Fe^{2+} and Fe^{3+} labile pools in live plants, we have established a method combining 2 probes, which enables specific detection of the redox state of the labile Fe pools.

To that aim, we have selected 2 fluorescent probes, SiRhoNox-1 (Hirayama et al. 2017) and MPNBD (Park et al. 2014), which we used to image labile Fe^{2+} and Fe^{3+}, respectively, in Arabidopsis (*Arabidopsis thaliana*) roots (Supplementary Methods). The 2 probes were chosen in such a way that their spectral properties do not overlap, allowing their simultaneous utilization without any cross-talk (Supplementary Fig. S1). The specificity of each probe was reconfirmed in vitro albeit in an aqueous buffer adapted for plant applications (Supplementary Fig. S2). The fluorescence of the 2 probes, though depending on pH, was found rather stable at physiological pH (6.0 to 6.5; Supplementary Fig. S2, G and H). Fluorescence intensity fluctuations must therefore be interpreted cautiously. The selectivity of the probes toward the redox state of Fe was tested by applying them to various Fe species in vitro. The mixed probes detected labile Fe species (Fe(II)-acetate, Fe(II)-SO_4, Fe(III)-NO_3, and Fe(III)-Cl_3), but not the Fe species involved in strong chelates such as EDTA or citrate (Fig. 1A). In vitro ascorbate-mediated reduction of Fe^{3+} species into Fe^{2+} was successfully monitored by the probes (Fig. 1B), suggesting that the method is suitable to assess reductase activity in vivo.

SiRhoNox-1 and MPNBD were applied in combination to 7-d-old plants and compared with Perls-DAB staining (Fig. 1, C to K). The fluorescent signals observed with the 2 probes were heterogeneously distributed along the entire primary root and were distinct from each other (Supplementary Fig. S3). Three root zones representative of the distribution of Fe^{2+} and Fe^{3+} were observed at higher magnification (Fig. 1, D, G, and J). Fe^{3+} was markedly predominant in the primary root apex (Fig. 1J) but absent in the young lateral root (Supplementary Fig. S4, A to C). Likewise, Perls-DAB did not stain the emerging root, suggesting that if Fe is present at this stage, its level is under the detection threshold of the 2 methods (Supplementary Fig. S4D). The primary root apex exhibited no Fe^{2+} signal (Fig. 1J). In contrast, in the differentiation zone, a strong Fe^{2+} fluorescent signal was observed at the cell periphery (Fig. 1G), suggesting an apoplastic localization. This observation is in agreement with previous studies reporting elemental analyses of cellular fractions (Bienfait et al. 1985; Ye et al. 2015; Liu et al. 2023). Plasmolysis of root cells confirmed the apoplastic localization of Fe^{2+} (Supplementary Fig. S5). Moreover, colocalization of FM4-64 and SiRhoNox-1 revealed the presence of Fe^{2+} at the plasma membrane (Supplementary Fig. S5F). 3D images of each root zone emphasized the variation of distribution of the 2 Fe redox species between cell layers and according to root age (Supplementary Fig. S6).

The Fe redox imaging method was applied to the Fe homeostasis ferric reduction oxidase 2 mutant (*fro2*), the Fe^{3+}/Fe^{2+} ratio of which is imbalanced owing to a loss of its ability to reduce Fe^{3+} at the root surface (Robinson et al. 1999; Connolly et al. 2003). Compared to wild type, the differentiation and mature zones of the *fro2* root expectedly exhibited a dramatic decrease of fluorescence with SiRhoNox-1, confirming the specificity of the SiRhoNox-1 probe for Fe^{2+} in vivo (Fig. 1, E and H, Supplementary Fig. S7). The penetration ability of the probes was examined using confocal microscopy. Fluorescence of SiRhoNox-1 and MPNBD was visible in most layers of the root including the vascular cylinder (Fig. 2, A to E), indicating that the 2 probes are able to penetrate all the tissues of the root. In addition, fluorescence signals of the Fe probes were detected inside the cells, showing the permeability of the plasma membrane toward these probes. In epidermal cells, MPNBD fluorescence filled the symplast (Fig. 2, F and H), whereas SiRhoNox-1 fluorescence surrounded the cells (Fig. 2G). Upon Fe limitation, SiRhoNox-1 produced intracellular punctuate signals (Fig. 2, I and J; Hirayama et al. 2013, 2017). Interestingly, the method highlighted a polarized pattern of Fe^{2+} at the external side of epidermal cells in the differentiation zone (Fig. 2, K to M), a feature that had not been reported previously. Such Fe^{2+} polarization is reminiscent of the polar localization of

Received December 11, 2023. Accepted March 20, 2024.

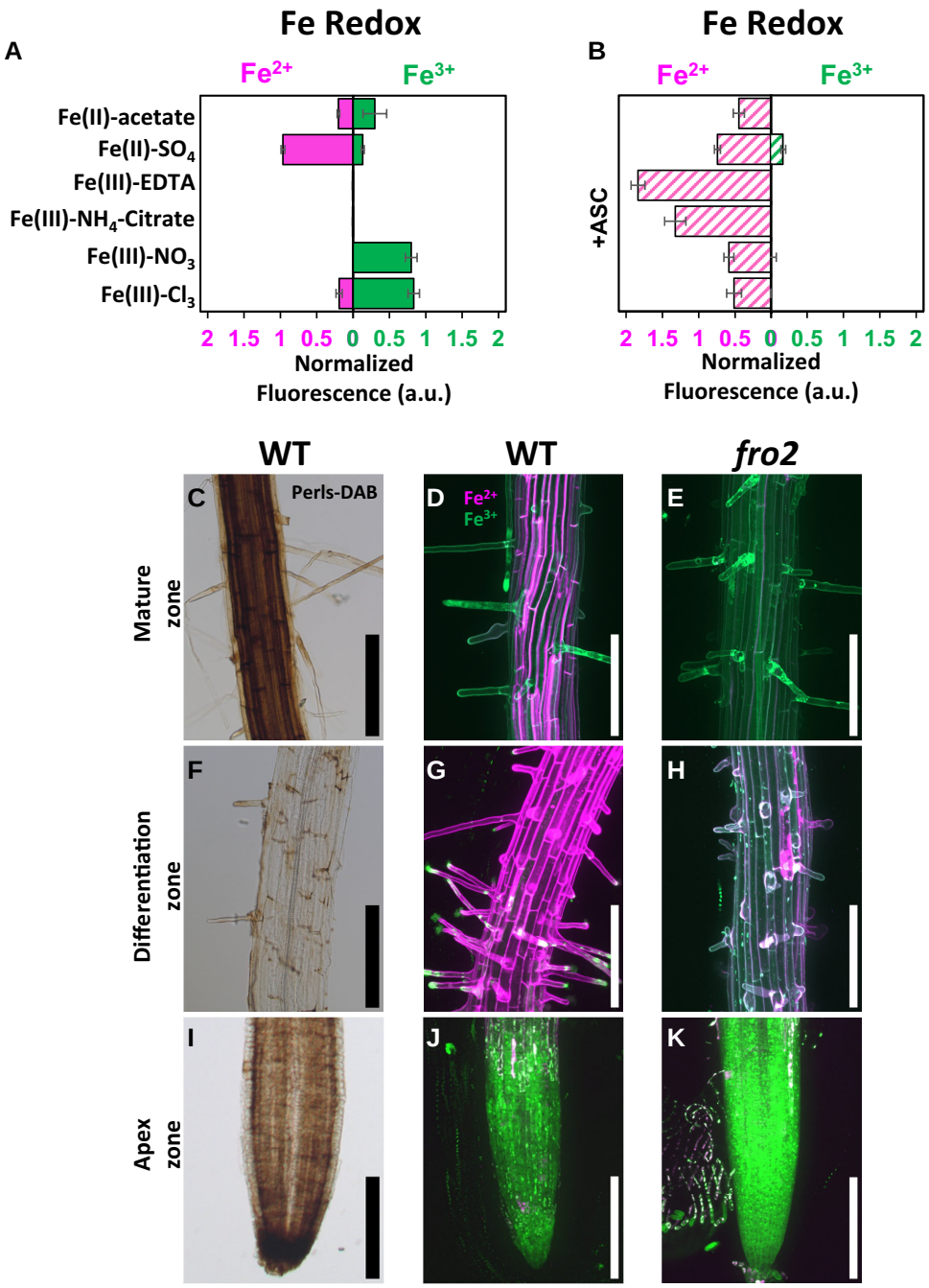

Figure 1. In vitro and in vivo detection of labile Fe^{2+} and Fe^{3+} using fluorescent probes. **A, B)** Determination of the specificity of the SiRhoNox-1 and MPNBD probes in vitro. **A)** Both probes were applied in combination to 1 mM solutions of a variety of Fe species. **B)** Reduction of Fe^{3+} by addition of 1 mM ascorbate (ASC) to the different Fe species allowed detecting a change of Fe redox state. **C to K)** In vivo imaging of Fe in the roots of 7-d-old Arabidopsis plants grown on 0.5xMS containing 50 μM Fe-EDTA. Labile Fe, detected using combined SiRhoNox-1 and MPNBD **D**, **E, G, H, J, K)**, was compared with Fe histochemical staining with the Perls-DAB method **C, F, I)**. In the primary root, the mature zone **C to E)**, differentiation zone **F to H)**, and apex zone **I to K)** are shown. The projection of maximum intensity of the Z-stack of fluorescent pictures is shown for SiRhoNox-1 (Fe^{2+}, magenta LUT) and MPNBD (Fe^{3+}, green LUT) in wild-type (WT) plants **D, G, J)** and in the *fro2* mutant **E, H, K)**. Data shown are mean ± SD. Data were collected from 3 to 4 independent experiments. a.u., arbitrary unit; DAB, 3,3′-diaminobenzidine. All scale bars = 200 μm.

FRO2 in the same cell type (Martín-Barranco et al. 2020). Remarkably, this polar distribution shifted to the inner side of the epidermal cells in the mature zone (Fig. 2, compare K-O and P-T) where Fe^{2+} was observed in the apoplast (Fig. 2T, red arrows). Quantification of the fluorescence signals allowed detecting subtle changes in the balance between Fe states, as shown in Fe-sufficient and Fe-deficient conditions in wild type and the *fro2* mutant (Supplementary Fig. S7).

In summary, combining fluorescent probes for Fe^{2+} and Fe^{3+} represents an original method to distinguish the redox species of Fe within live tissues, reveals their distribution in root, and uncovers a remarkable polarization of Fe^{2+}. Because this method can detect subtle differences of Fe charges in the tissues, it will become useful to characterize actors of the redox status of Fe, such as oxidoreductases, hence equipping the community with a powerful tool to explore Fe homeostasis in plants.

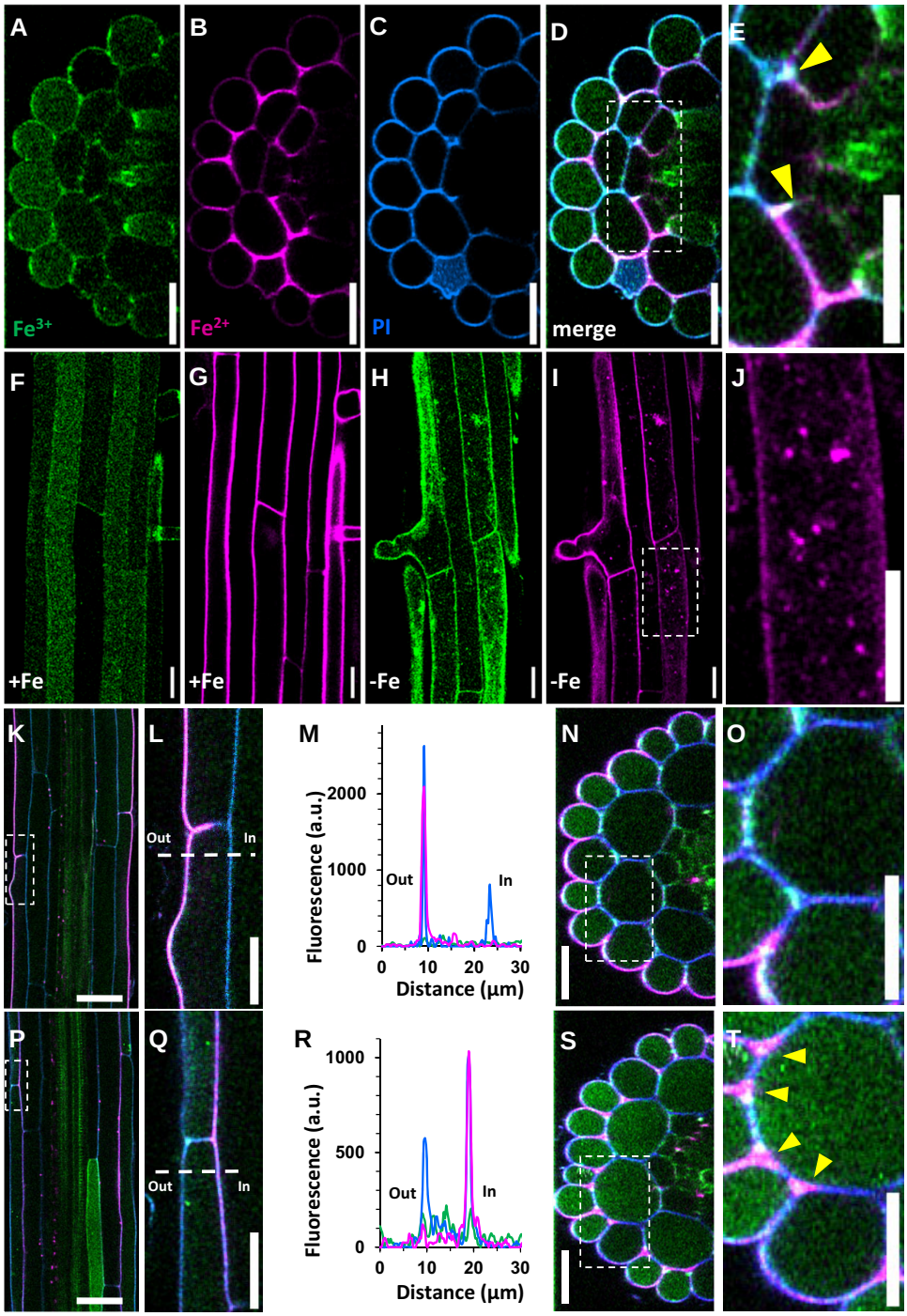

Figure 2. Distribution of labile Fe in the different cell layers of the primary root of *A. thaliana*. Images were taken from 7-d-old seedlings. **A to E)** Representative orthogonal view of the mature zone of the primary root stained with MPNBD (Fe^{3+}, **A**), SiRhoNox-1 (Fe^{2+}, **B**), propidium iodide (cell wall, **C**), or a merged image of the 3 probes **D, E)**. Labile Fe^{2+} and Fe^{3+} are present in most cell types with a signal in the endodermis. An enlarged view of the endodermal layer indicated by a dashed square shows interruption of the apoplastic fluorescent signal at the Casparian strip (arrowheads, **E**). **F to J)** MPNBD and SiRhoNox-1 fluorescent signals in root epidermis showing the presence of Fe^{3+} inside the cell **F)** and Fe^{2+} in the apoplast **G)** of Fe-replete plants as well as in intracellular dot-like structures of Fe-deficient plants **H to J)**. **J)** Close-up view of the Fe^{2+} dots presented in **I)**. **K to T)** Polar distribution of Fe^{2+} in the epidermal cell wall. Differentiation **K to O)** and mature **P to T)** zones of the primary root were observed in longitudinal sections. Higher magnification of the epidermal cells **L, Q)** shows polar localization of Fe^{2+}, albeit in opposite pattern in the 2 zones, which is confirmed by the line profile of the fluorescence intensity of the probes **M, R)**. **N**, **S**, **O, T)** Orthogonal view of the differentiation **N, O)** and mature **S, T)** root zones, including the corresponding enlarged views **O, T)** indicated by dashed areas within **N) and S)**. **T)** SiRhoNox-1 labels the intercellular space in the mature zone (red arrows). **A to G** and **K to T)** Seedlings were grown on 0.5xMS containing 50 µM Fe-EDTA (+Fe). **H to J)** Seedlings were grown on 0.5xMS without Fe (–Fe). Magenta LUT: SiRhoNox-1; green LUT: MPNBD; BIOP-Azure LUT: propidium iodide. MPNBD, 7-(4-methylpiperazin-1-yl)-4-nitrobenzo-2-oxa-1,3-diazole; a.u., arbitrary unit. All scale bars = 20 µm.

Acknowledgments

We acknowledge the MRI imaging facility, member of the France-BioImaging national infrastructure supported by the French National Research Agency (ANR-10-INBS-04, "Investments for the future"), and PHIV-La Gaillarde facility.

Author contributions

C.A. and T.C.X. performed fluorescence imaging and Perls-DAB staining and designed and carried out the experiments. A.C. performed fluorescent probe synthesis. C.A., T.C.X., and C.C. wrote the paper.

Supplementary data

The following materials are available in the online version of this article.

Supplementary Figure S1. Excitation and emission spectra of SiRhoNox-1 and MPNBD probes at pH 6.0.

Supplementary Figure S2. In vitro characterization of the Fe redox SiRhoNox-1 and MPNBD fluorescent probes.

Supplementary Figure S3. Distribution of Fe along the primary root of *A. thaliana* grown on 0.5xMS containing 50 μM Fe-EDTA.

Supplementary Figure S4. The lateral root apex is not stained by the two Fe probes.

Supplementary Figure S5. Fe is localized in the apoplastic space of root epidermal cells.

Supplementary Figure S6. Differential spatial distribution of Fe^{2+} and Fe^{3+} according to the developmental stage of the root in 7-d-old plants grown in Fe-replete conditions.

Supplementary Figure S7. Changes in Fe redox state are dependent on growth conditions and Fe homeostasis.

Supplementary Methods.

Funding

This work was supported by the National Research Institute for Agricuture, Food and the Environment (INRAE) grant BAP 2020 "FluoMet" and the National Centre for Scientific Research (CNRS) grant Mission pour les Initiatives Transverses et Interdisciplinaires Metallomix 2021 "DESCIFERMAN."

Conflict of interest statement. None declared.

Data availability

The data underlying this article will be shared on reasonable request to the corresponding author.

References

Bienfait HF, Van Den Briel W, Mesland-Mul NT. Free space iron pools in roots: generation and mobilization. *Plant Physiol*. 1985:78(3):596–600. https://doi.org/10.1104/pp.78.3.596

Briat J-F, Dubos C, Gaymard F. Iron nutrition, biomass production, and plant product quality. *Trends Plant Sci*. 2015:20(1):33–40. https://doi.org/10.1016/j.tplants.2014.07.005

Connolly EL, Campbell NH, Grotz N, Prichard CL, Guerinot ML. Overexpression of the FRO2 ferric chelate reductase confers tolerance to growth on low iron and uncovers posttranscriptional control. *Plant Physiol*. 2003:133(3):1102–1110. https://doi.org/10.1104/pp.103.025122

Hirayama T, Okuda K, Nagasawa H. A highly selective turn-on fluorescent probe for iron(II) to visualize labile iron in living cells. *Chem Sci*. 2013:4(3):1250. https://doi.org/10.1039/c2sc21649c

Hirayama T, Tsuboi H, Niwa M, Miki A, Kadota S, Ikeshita Y, Okuda K, Nagasawa H. A universal fluorogenic switch for Fe(II) ion based on N-oxide chemistry permits the visualization of intracellular redox equilibrium shift towards labile iron in hypoxic tumor cells. *Chem Sci*. 2017:8(7):4858–4866. https://doi.org/10.1039/C6SC05457A

Koppenol WH, Hider RH. Iron and redox cycling. Do's and don'ts. *Free Radic Biol Med*. 2019:133:3–10. https://doi.org/10.1016/j.freeradbiomed.2018.09.022

Liu XX, Zhu XF, Xue DW, Zheng SJ, Jin CW. Beyond iron-storage pool: functions of plant apoplastic iron during stress. *Trends Plant Sci*. 2023:28(8):941–954. https://doi.org/10.1016/j.tplants.2023.03.007

Martín-Barranco A, Spielmann J, Dubeaux G, Vert G, Zelazny E. Dynamic control of the high-affinity iron uptake complex in root epidermal cells. *Plant Physiol*. 2020:184(3):1236–1250. https://doi.org/10.1104/pp.20.00234

Park M-J, Jung H-S, Kim Y-J, Kwon Y-J, Lee J-K, Park C-M. High-sensitivity fluorescence imaging of iron in plant tissues. *Chem Commun*. 2014:50(62):8547–8549. https://doi.org/10.1039/C4CC02132K

Robinson NJ, Procter CM, Connolly EL, Guerinot ML. A ferric-chelate reductase for iron uptake from soils. *Nature* 1999:397(6721):694–697. https://doi.org/10.1038/17800

Roschzttardtz H, Conéjéro G, Curie C, Mari S. Identification of the endodermal vacuole as the iron storage compartment in the Arabidopsis embryo. *Plant Physiol*. 2009:151(3):1329–1338. https://doi.org/10.1104/pp.109.144444

Ye YQ, Jin CW, Fan SK, Mao QQ, Sun CL, Yu Y, Lin XY. Elevation of NO production increases Fe immobilization in the Fe-deficiency roots apoplast by decreasing pectin methylation of cell wall. *Sci Rep*. 2015:5(1):10746. https://doi.org/10.1038/srep10746